Environmental Pollution 271 (2021) 116379

Contents lists available at ScienceDirect

Environmental Pollution

journal homepage: www.elsevier.com/locate/envpol

Pre-differentiation exposure to low-dose of atrazine results in persistent phenotypic changes in human neuronal cell lines☆

Junkai Xie [a], Li Lin [a, 1], Oscar F. Sánchez [b], Chris Bryan [c], Jennifer L. Freeman [d, e], Chongli Yuan [a, e, *]

[a] Davidson School of Chemical Engineering, Purdue University, West Lafayette, IN, 47907, USA
[b] Department of Nutrition and Biochemistry, Pontificia Universidad Javeriana, Bogotá, 110231, Colombia
[c] Department of Statistics, Purdue University, West Lafayette, IN, 47907, USA
[d] School of Health Sciences, Purdue University, West Lafayette, IN, 47907, USA
[e] Purdue University Center for Cancer Research, West Lafayette, IN, 47907, USA

ARTICLE INFO

Article history:
Received 23 September 2020
Received in revised form
4 December 2020
Accepted 21 December 2020
Available online 23 December 2020

ABSTRACT

Exposures to organic pesticides, particularly during a developmental window, have been associated with various neurodegenerative diseases later in life. Atrazine (ATZ), one of the most used pesticides in the U.S., is suspected to be associated with increased neurodegeneration later in life but few studies assessed the neurotoxicity of developmental ATZ exposure using human neuronal cells. Here, we exposed human SH-SY5Y cells to 0.3, 3, and 30 ppb of ATZ prior to differentiating them into dopaminergic-like neurons in ATZ-free medium to mimic developmental exposure. The differentiated neurons exhibit altered neurite outgrowth and SNCA pathology depending on the ATZ treatment doses. Epigenome changes, such as decreases in 5mC (for 0.3 ppb only), H3K9me3, and H3K27me3 were observed immediately after exposure. These alterations persist in a compensatory manner in differentiated neurons. Specifically, we observed significant reductions in 5mC and H3K9me3, as well as, an increase in H3K27me3 in ATZ-exposed cells after differentiation, suggesting substantial chromatin rearrangements after developmental ATZ exposure. Transcriptional changes of relevant epigenetic enzymes were also quantified but found to only partially explain the observed epigenome alteration. Our results thus collectively suggest that exposure to low-dose of ATZ prior to differentiation can result in long-lasting changes in epigenome and increase risks of SNCA-related Parkinson's Disease.

1. Introduction

Atrazine (ATZ; 2-chloro-4-(ethylamino)-6-(isopropylamino)-s-triazine) is one of the most commonly used pesticides in the United States with an estimated annual use of ~70 million pounds (P. Gianessi and B. Marcelli, 2000). High concentrations of ATZ (>30 ppb) are commonly detected in surface water and deep wells in agricultural regions of the U.S., such as Indiana, Ohio, and California (Raja et al., 2005) due to its good water solubility (34.7 mg/L) and relative long half-life (>200 days) (Cheremisinoff 2011). Exposure to ATZ, particularly in agriculture workers, has been associated with increased risk of various diseases, including breast cancers (Simpkins et al., 2011), reproductive and endocrine diseases (Munger et al., 1997), and neurodegenerative diseases (Song et al., 2015). The molecular mechanism of neurotoxicity of ATZ, however, is not as well studied.

Exposure to low dose of ATZ can cause aberrant alterations in neurological systems as shown in fish and rodent models. Specifically, exposure to ATZ in adult mice can induce multiple behavioral abnormalities involving motor, cognitive and emotional functions (Giusi et al., 2005; Lin et al., 2013a, 2013b). In male mice, several neurotransmitters and their metabolites including dopamine and serotonin were significantly increased in striatum, prefrontal cortex and hippocampus after short-term exposure to low-dose of ATZ. These findings indicate that ATZ targets multiple monoamine pathways in different brain regions to induce behavioral abnormalities (Lin et al., 2013a, 2013b). In female mice, ATZ induced

☆ This paper has been recommended for acceptance by Wen Chen.

* Corresponding author. Davidson School of Chemical Engineering, Purdue University, West Lafayette, IN, 47907, USA.
E-mail address: cyuan@purdue.edu (C. Yuan).
[1] Current address: Department of Chemical and Biomolecular Engineering, University of California, Berkeley, CA 94704,USA.

https://doi.org/10.1016/j.envpol.2020.116379
0269-7491/

similar neuronal damages but with more extensive changes found in the hippocampal and hypothalamic area (Giusi et al., 2005). Similar observations were made in rat and fish models, such as alternations in motor function and social behavior (Schmidel et al., 2014; Song et al., 2015; Walters et al., 2015). Transcriptomic studies using rat models further revealed changes in gene expression after ATZ exposure. Dopamine metabolism pathways associated with dopaminergic system development are significantly altered after ATZ exposure in both sex (Sun et al., 2014; Li et al., 2015).

Developmental exposure to ATZ was shown to have more severe toxicity on the central nervous system (CNS) compared to adult exposure. For example, in a rodent model, developmental exposure to ATZ can result in significant changes in the activity of dopaminergic neurons via altering the expression of D1 dopamine receptor (*D1DR*), *PKA*, and *BDNF* (Coban and Filipov 2007). The exposed rats exhibited reductions in spatial learning and memory capacity as well as locomotor activities (Coban and Filipov 2007; Walters et al., 2015). In zebrafish, embryonic exposure to ATZ caused significant changes in genes associated with movement disorders, i.e., *AQP1*, *CDK5*, and *TNNI2* that are associated with dopaminergic systems (Horzmann et al., 2020). The exposed fish also exhibited anxiety-like behavior, such as changes in movement time, location and velocity (Horzmann et al., 2020). It is noteworthy that the behavior and transcriptomic changes caused by ATZ in animal models partially resembles the pathology of Parkinson's Disease (PD). Although alterations in the expression of neurotransmitter receptors, such as D1 Dopamine Receptor (*D1DR*) and serotonin receptors *HTR2C* and *HTR1A* (Coban and Filipov 2007; Wirbisky et al., 2015; Horzmann et al., 2020), can partially explain ATZ-induced neurotoxicity, the observed changes in transcriptome do not necessarily persist and tend to be restored after the cessation of exposure to ATZ suggesting the involvement of an upstream regulatory mechanism.

Exposure to ATZ does not only affect the exposed generation, but also its progeny (Hao et al., 2016; McBirney et al., 2017). For example, the first generation of ATZ-exposed mice (F0) showed compromised motor functions and anxiety-like symptoms along with significant alterations in the expression of genes enriched in metabolic and endocytosis pathways (Lin et al., 2014; McBirney et al., 2017). Strikingly, their offspring exhibit similar changes in both gene expression and behavior. These results provide strong evidence of the involvement of an inheritable mechanism conferring ATZ-induced neurotoxicity. Since low-dose ATZ is known to have low-to non-mutagenetic activity, epigenetic mechanism is thus heavily implied as one of the underlying mechanisms.

Epigenetics, include DNA methylation, histone post-translational modifications and noncoding RNAs, is the study of the molecular mechanisms that regulate gene expression without alternating the innate DNA sequence and is the bridge between genotype and phenotype (Goldberg et al., 2007). DNA methylation, particularly promoter methylation is commonly involved in gene repression. The roles of histone post-translational modifications on gene expression are more diverse and range from gene activation (e.g., H3K4me3 (Wysocka et al., 2006)), facultative gene repression (H3K27me3 (Wiles and Selker 2017)) to permanent gene silencing (e.g., H3K9me3 (Mozzetta et al., 2015)). Exposure to ATZ is known to alter epigenome and epigenetic enzyme activity. In the trans-generation mice study, ATZ-exposed mice showed persistent alterations in DNA methylation and H3K4me3 that last to the third generation (F3) (Hao et al., 2016; McBirney et al., 2017). Specifically, ATZ-exposed rats and their offspring shared similar differential methylated regions (DMR) that were enriched in endocytosis and neuroactive ligand-receptor pathway for three and one generation, respectively (McBirney et al., 2017). Significant decrease in H3K4me3 were observed up to the third generation of ATZ-exposed mice via altering the expression of *Kdm5b*, a lysine demethylase for H3K4me3 (Hao et al., 2016). Similar DNA methylation alterations were found in zebrafish and human cell lines exposed to ATZ (Wirbisky-Hershberger et al., 2017; Sánchez et al., 2019; Sánchez et al., 2020). Furthermore, ATZ can work as a non-competitive inhibitor for DNA methyltransferases (DNMTs) (Wirbisky-Hershberger et al., 2017) and thus affect their reactivity. Exposure to ATZ is also associated with expression changes in DNMT in zebrafish and human cell line studies (Sánchez et al., 2019; Sánchez et al., 2020).

Alterations in epigenome are also commonly observed in various neurodegenerative diseases, and thus, provide a plausible connection bridging exposure to ATZ and neurotoxicity. Genome-wide methylation analysis in PD patients revealed significant DNA methylation changes between cases and controls with changes most significant in DNA methylation valleys (Young et al., 2019). Imputation of DNA methylation levels in the brain has also been suggested as a potential predictive marker of PD risk (Rawlik et al., 2016). Although many review papers have suggested the potential role of histone post-translational modifications on PD (Wen et al., 2016), few studies explicitly studied changes in histone post-translational modifications of PD brains except for histone acetylation (Gebremedhin and Rademacher 2016; Park et al., 2016).

Collectively, current literature suggest that epigenome changes induced by exposure to ATZ can work as a potential "memory" that records past exposure events, persists, and later increases the risk of neurodegenerative diseases. The epigenetic mechanism conferring ATZ-induced neurotoxicity and the nature of persistency, however, remains elusive. To elucidate the epigenetic mechanism of ATZ neurotoxicity and assess the persistency of various epigenetic markers, we used a model human cell line SH-SY5Y in this work. We exposed SH-SY5Y cells to varying doses of ATZ prior to differentiation mimicking developmental exposure. Phenotypic and epigenetic assessments were carried out to reveal the impact of ATZ-exposure and validate the role of epigenetic mechanism in conferring ATZ neurotoxicity.

2. Materials and methods

2.1. Culture and differentiation of SH-SY5Y cells

Human neuroblastoma SH-SY5Y cells (ATCC: CRL-2266™, USA) were grown in Eagle's Minimum Essential Medium supplemented with 50% nutrient mixture F-12 (EMEM/F-12, Gibco, USA), 10% fetal bovine serum (Atlanta Bio., USA), 1× of penicillin-streptomycin (P/S, Life Technologies, USA) and 1× of MEM Non-Essential amino acids (Gibco, Life Technologies, USA). Cultures were maintained at 37 °C in humidified air with 5% CO_2, with a medium change every two days. Cells below passage number of 15 were used in all studies.

SH-SY5Y cells can be differentiated into dopaminergic neurons following an established protocol (Shipley et al., 2016) and is commonly used for studying neurodegeneration, particularly Parkinson's Disease (PD) (Xie et al., 2010; Xicoy et al., 2017). Briefly, differentiation was initiated in a Differentiation Medium 1 containing EMEM, FBS, P/S and retinoic acid for 6 days followed by a medium exchange into Differentiation Medium 2 containing neural basal medium, B-27, BDNF, db-cAMP, P/S and retinoic acid for 8 days. The detailed composition of Differentiation Medium 1 and 2 were listed in Table S1 (Supporting Information). All cells were treated with varying doses of ATZ prior to starting the differentiation as illustrated in Fig. 1.

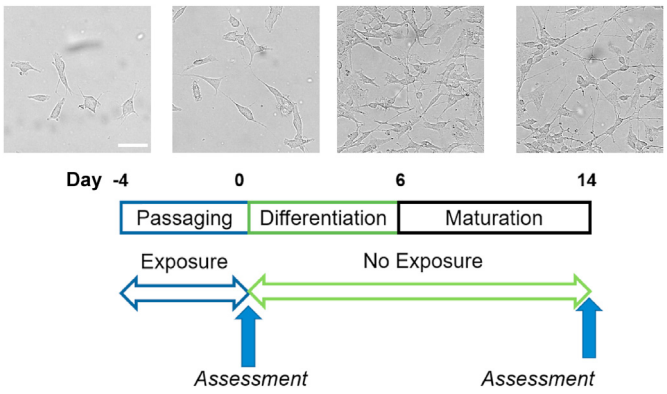

Fig. 1. A schematic illustration of atrazine exposure and neuron differentiation timeline for SH-SY5Y cell line. Representative brightfield images of SH-SY5Y cells are shown above their respective time points. Scale bar = 50 μm.

2.2. Atrazine treatment

All cells were treated with varying doses of ATZ for 4 days (96 h) prior to differentiation. In addition to the control (0 ppb), we used ATZ concentrations of 0.3, 3 and 30 ppb. The exposure duration was selected based on the doubling time of SH-SY5Y cells (~48 h) to ensure at least one round of cell replication during the exposure window. The dose of ATZ exposure were selected based on the current EPA regulation standard (3 ppb) and past studies that suggest 30 ppb as the minimal doses of ATZ that can elicit gene expression changes while having minimal effects on cell/animal viability (EPA. 2002; Rohr and McCoy 2010). Although higher doses of ATZ have been reported in surface water and topsoil (Raja et al., 2005; Vonberg et al., 2014), we selected to work with low-dose of ATZ given their likely prevalence in our living environment. ATZ solution was prepared from a stock solution as described previously (Wirbisky et al., 2015); and was then spiked into culture medium. All cells were treated for a total duration of 96 h with a medium exchange every 48 h. After 96 h, ATZ-containing medium was aspirated. Cells were then washed three times using passaging medium before starting the differentiation.

2.3. Immuno-staining

All cells were fixed in 4% formaldehyde (Thermo Fisher, USA) and permeabilized using 1% Triton-X (Millipore-Sigma, USA) following our established protocol (Sánchez et al., 2019). Primary antibodies used in this study were anti-DNA methylation (Active Motif, 61479), anti-H3K9me3 (Abcam, ab8898), anti-H3K27me3 (Abcam, ab192985), anti-α-synuclein (Invitrogen, 328100) and anti-A11 oligomer (Invitrogen, AHB0052). For DNA methylation staining, an additional denaturation step was included to dissociate DNA for binding to the primary antibody as we described previously (Lin et al., 2020). Secondary antibodies, including anti-mouse Alexa 568 (Invitrogen, A11004) and anti-rabbit Alexa 568 (Abcam, ab175471) were used.

2.4. Fluorescence microscopy

All fluorescence microscopy images were collected using Nikon Eclipse Ti-2 inverted microscope with 60× /1.40 Plan Apo Vc oil objective or a high-throughput imaging platform (ImageXpress Micro Confocal, Molecular Device) with Nikon 10× /0.5 Plan Apo and 20× /0.75 Plan Apo Lambda objectives. All images were analyzed using a customized CellProfiler pipeline (Broad Institute, U.S.) for feature extraction and quantification. Neurite outgrowth were analyzed using a neurite analysis module in MetaXpress (Molecular Device, California).

2.5. Assess α-synuclein aggregates via co-exposing to known neurotoxins

MPP+ and dopamine are known risk factors for PD (Chun et al., 2001). Dopamine can increase the expression of α-synuclein, while MPP+ can facilitate the aggregation of α-synuclein (Yamakawa et al., 2010). To assess the risk of PD-pathogenesis, specifically α-synuclein aggregates, all differentiated SH-SY5Y cells were treated with 100 μM of dopamine for 18 h followed by the addition of 750 nM of MPP+ for 6 h. Cells were then fixed and stained for α-synuclein aggregates using anti-A11 oligomer antibody (Invitrogen, AHB0052) as primary.

2.6. RT-qPCR

Total RNA was extracted from cell pellets using a PureLink RNA Extraction kit (Invitrogen, USA) following the manufacturer's protocol. RT-qPCR was performed similarly as we described previously (Lin et al., 2020). Briefly, 1 μg of RNA were converted to cDNA using SuperScript IV Reverse Transcriptase (Invitrogen, USA) and random hexamers (IDT DNA, USA). qPCR was then performed using PowerUp SYBR mixture (Invitrogen, USA), and the housekeeping gene β-actin was used as the endogenous control. The sequence of all primers used in this study was summarized in Table S2 (Supporting Information). *Ct* values were determined using 3–4 biological replicates, each with 3 technical repeats. Δ*Ct* was calculated using *β*-actin as the reference. Significant difference in Δ*Ct* was determined using ANOVA followed by Fisher's LSD post-hoc test ($p < 0.05$).

2.7. Statistical analysis

Three independent replications of the experiments were performed with a minimum of three biological replicates. Data were initially subjected to an analysis of variance (ANOVA) to determine the significance of treatment effects. *p*-value was calculated using Fisher LSD post-hoc test and $p < 0.05$ was considered as statistically significant. Principle component analysis (PCA), t-Distributed Stochastic Neighbor Embedding (t-SNE) and k-mean clustering analysis was performed using R-studio.

3. Results

3.1. Exposure to low-dose of ATZ induces phenotypical alterations in differentiated SH-SY5Y

SH-SY5Y cells were exposed to selected doses of ATZ, namely 0, 0.3, 3, and 30 ppb, for 96 h prior to differentiation following the scheme in Fig. 1. The exposure doses were selected based on the current U.S. EPA regulation standard (EPA. 2006), as well as, prior atrazine studies (Wirbisky et al., 2015; Wirbisky-Hershberger et al., 2017). We characterized SH-SY5Y viability at the selected concentrations via an MTT assay. All cells were treated for 96 h before assessment. We found that ATZ has low to no cytotoxic effects on SH-SY5Y cells at the selected doses as shown in Fig. S1 (Supporting Information).

SH-SY5Y cells in an undifferentiated state have been commonly used for neurotoxicity studies (Xie et al., 2010). SH-SY5Y cells can also be differentiated into dopaminergic-like neurons and thus commonly used as a cell line model for studying PD (Xicoy et al., 2017). Mature neurons differentiated from SH-SY5Y cells stain

positive for MAP2 (Shipley et al., 2016). Representative images of MAP2+ cells are shown in Fig. 2A. Pre-differentiation exposure to ATZ is found to be a significant factor in determining the percentage of MAP2 positive cells (MAP2+%) by ANOVA ($p < 0.05$). Significantly, increase in MAP2+% was observed for cells exposed to 30 ppb of ATZ as shown in Fig. 2B.

All differentiated neurons exhibit typical neuron morphology with elongated neurites. We quantified neurite growth by determining the neurite length and number of neurite branches using typical cell images as shown in Fig. S2A (Supporting Information). Compared to ATZ-naïve cells, ATZ treatment has resulted in a significant increase in neurite length for cells treated with 0.3 ppb of ATZ as shown in Fig. 2C. Moreover, the number of neurite branches characterizing the complexity of the connection between neurons is also altered by exposure to ATZ as shown in Fig. 2D. Specifically, cells exposed to 0.3 ppb of ATZ have significantly larger number of neurite branches compared to ATZ-naïve cells. Collectively, cells exposed to 0.3 ppb of ATZ exhibited the most significant changes in neurite outgrowth with longer neurite length and larger number of neurite branches. Cells exposed to 30 ppb of ATZ exhibited the largest change in differentiation efficiency manifested as increase in MAP2+%, We then evaluated changes in PD-related pathological markers, namely α-synuclein (*SNCA*) after the completion of neuron differentiation. Typical images of differentiated SH-SY5Y cells (Day 14) stained for α-synuclein are shown in Fig. 3A (see Fig. S2B (Supporting Information) for more images). *SNCA* expression is significantly enriched in neurites and the expression is the highest in cells treated with 3 ppb of ATZ, followed by cells exposed to 30 ppb of ATZ. RT-qPCR was performed to determine changes in the transcription of *SNCA* with results summarized in Fig. 3B. Differentiated SH-SY5Y cells (Day 14) have significantly higher levels of transcription of SNCA than undifferentiated cells (Day 0). At Day 0, ~11.9-, 2.7-, and 6.7-folds increase in SNCA transcription were observed for cells exposed to 0.3, 3, and 30 ppb of ATZ, respectively. At Day 14, after the completion of differentiation, ~2.5-fold increase in *SNCA* transcription is observed in cells exposed to 3 ppb of ATZ, while changes in cells exposed to other doses of ATZ have been almost completely restored.

Given the increase in *SNCA* transcription and expression, we further evaluated the risk of differentiated cells in developing synuclein aggregates. Exposure to ATZ does not immediately elicit *SNCA* aggregates. We thus treated cells with known PD risk factors, namely MPP+ and dopamine to facilitate the oligomerization of α-synuclein as demonstrated in literature (Yamakawa et al., 2010). Cells were subsequently fixed and stained with antibodies for Oligomer A11 with typical images summarized in Fig. 3C (see Fig. S2C (Supporting Information) for more images). These images were selected to have larger view areas to ensure the representativeness of our findings since A11 stains are not evenly distributed in different areas. The number of A11 stained dots remains almost unchanged in cells exposed to 0.3 and 3 ppb of ATZ. Significant increase in A11, however, can be observed in cells treated with 30 ppb of ATZ and the changes can be quantified as A11 intensity normalized to cell numbers which are summarized in Fig. 3D.

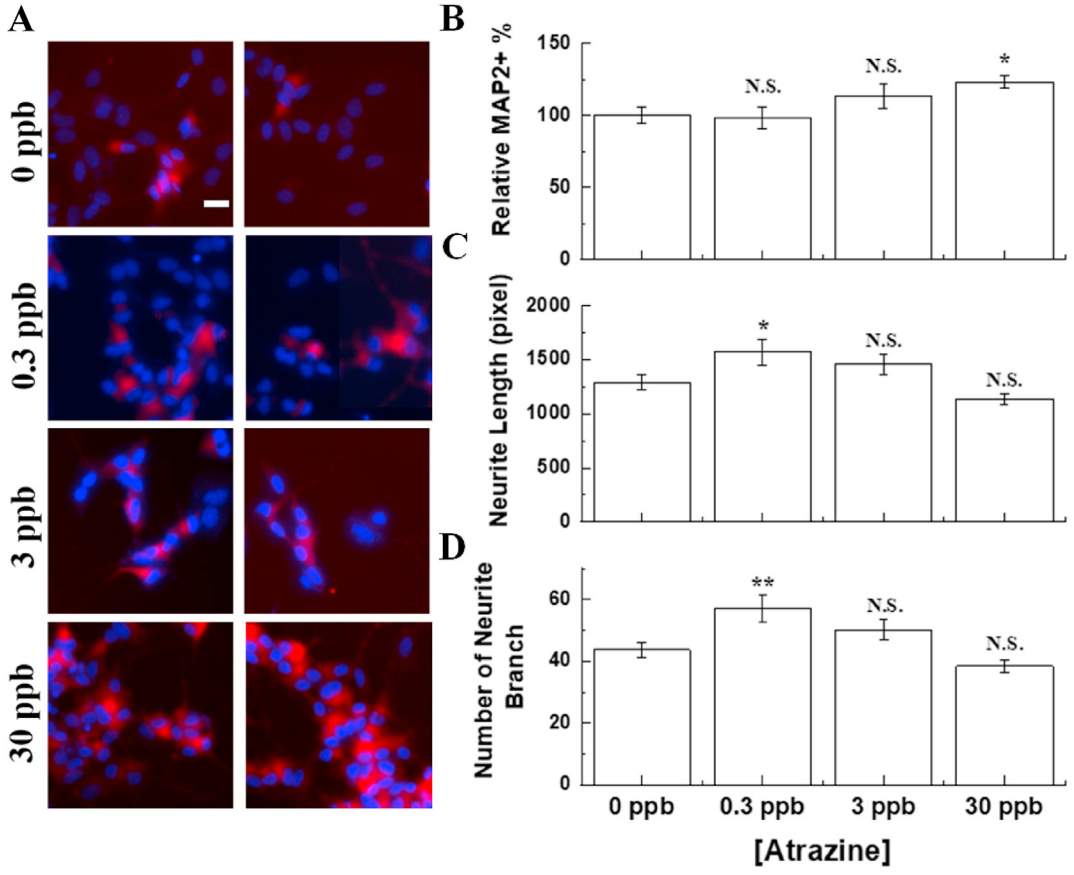

Fig. 2. A) 20x wide field images of SH-SY5Y cells stained for MAP2. Blue = DAPI, Red = MAP2. Scale bar = 10 μm. Changes in B) relative MAP2+% (normalized to untreated control); C) neurite length; and D) number of neurite branches in differentiated SH-SY5Y cells after exposure to ATZ of varying doses. n > 3 culturing wells, Data = mean ± S.E. *: $p < 0.05$, **: $p < 0.01$ and N.S.: not significant. (For interpretation of the references to colour in this figure legend, the reader is referred to the Web version of this article.)

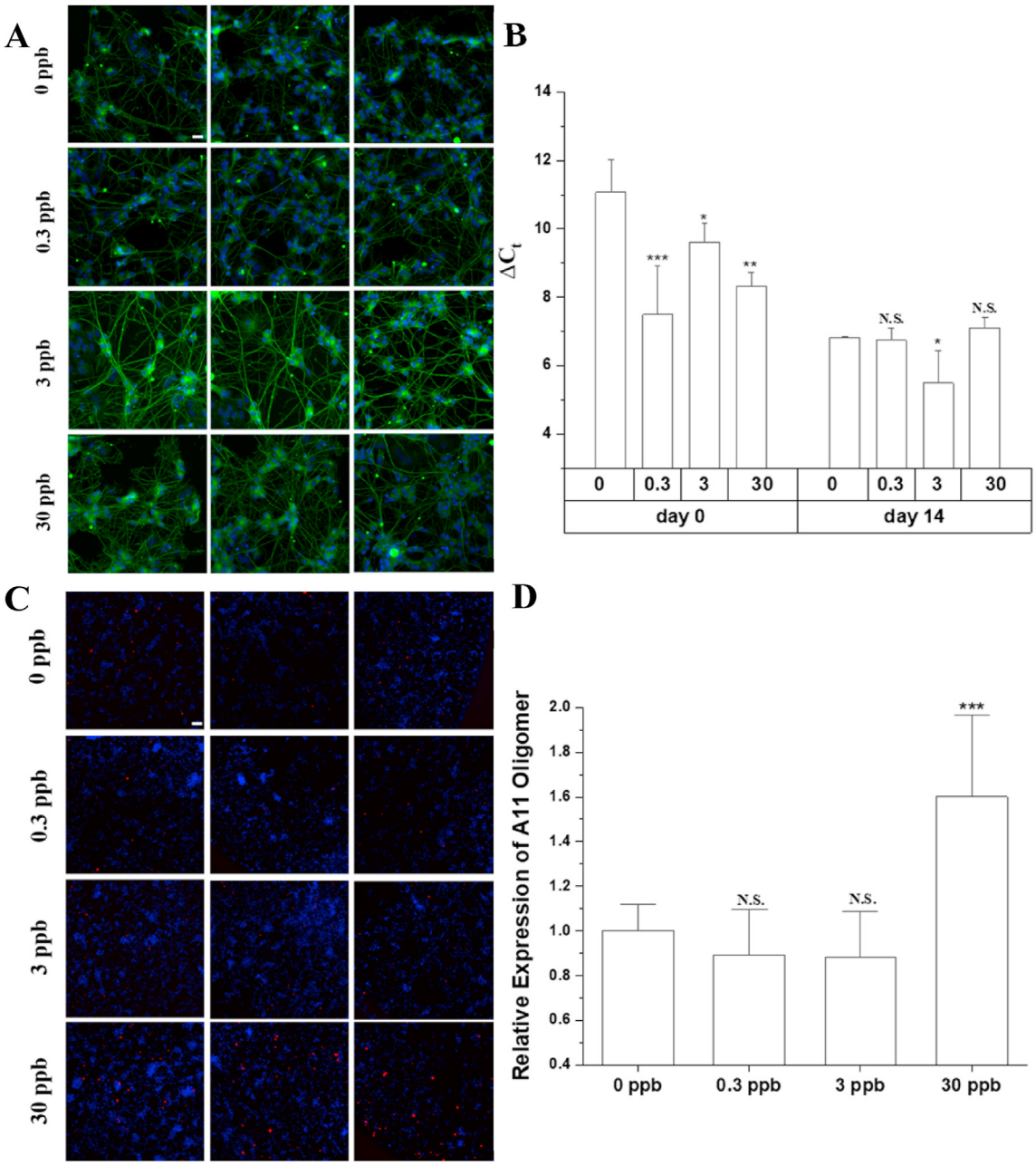

Fig. 3. A) Representative 20x wide-field images of differentiated SH-SY5Y cells (Day 14) stained for *SNCA*. Blue = DAPI, Green = α−synuclein. Scale bar = 20 μm. B) Transcription levels of *SNCA* mRNA assessed immediately after 96 h of exposure to ATZ (Day 0) and completion of differentiation (Day 14). Data are presented as the mean difference in threshold cycle (ΔC_t) between gene of interest and β-actin as internal control. Data = mean ± S.D. n = 3. C) Representative 10x wide-field images of differentiated SH-SY5Y cells (Day 14) stained for A11 oligomer. Blue = DAPI, Red = A11 Oligomer. Scale bar = 100 μm. D) Relative expression level of A11 oligomer at each treatment level. Data = mean ± S.D. n = 3. *: $p < 0.05$, **: $p < 0.01$, ***: $p < 0.001$ and N.S.: not significant. (For interpretation of the references to colour in this figure legend, the reader is referred to the Web version of this article.)

3.2. Exposure to low-dose of ATZ alters epigenome with changes persist through differentiation

Three types of epigenetic modifications, namely cytosine methylation (5mC), H3K9me3 and H3K27me3 are quantified immediately after exposure to ATZ (Day 0) and towards the completion of differentiation (Day 14) (see also Fig. 1). These modifications were selected because of their established roles in forming transcriptionally suppressed chromatin regions (Moore et al., 2013; Wiles and Selker 2017) and cell lineage determination (Nicetto and Zaret 2019).

After 96 h exposure to ATZ (Day 0), we obtained immunofluorescent images of SH-SY5Y cells as summarized in Fig. 4A–C with more images in Fig. S3 (Supporting Information). SH-SY5Y cells stained with 5mC exhibit bright foci enriched with 5mC islands inside nucleus and in the perinuclear area as shown in Fig. 4A (see Fig. S3A (Supporting Information) for more images). After ATZ exposure, 5mC intensity increased in cells exposed to 3 or 30 ppb of ATZ, suggesting an overall increase in 5mC levels. We calculated relative changes in 5mC based on the immunofluorescent intensity normalized to the untreated control (0 ppb). Our results show ~ −10, +20 and + 25% change in 5mC levels for cells

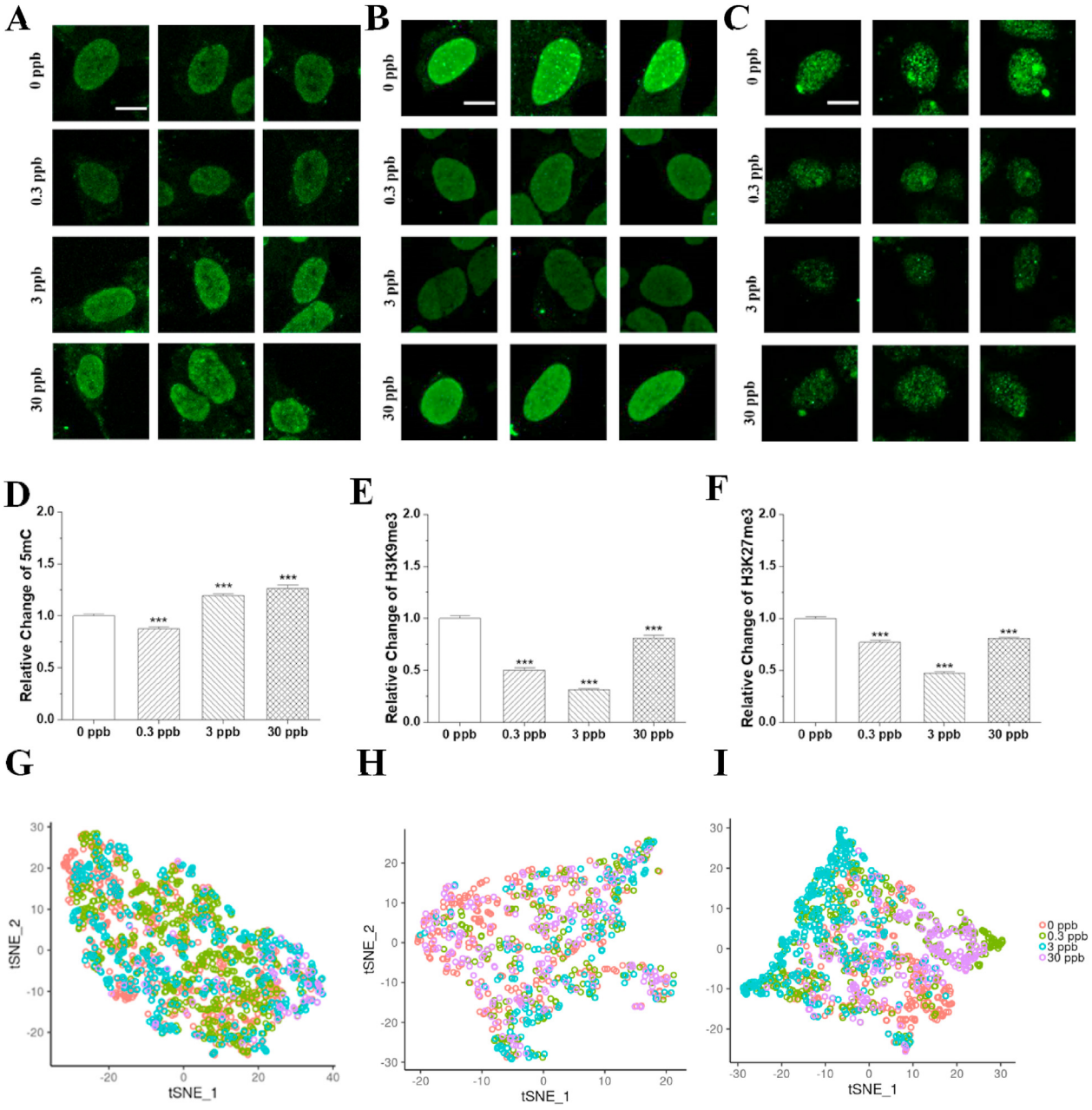

Fig. 4. (A–C) Typical confocal images (*z*-projected) of undifferentiated SH-SY5Y cells stained for (A) 5mC, (B) H3K9me3, and (C) H3K27me3 after 96 h exposure to ATZ. Scale bar = 5 μm. (D–F) Bar plots representing the relative change in (D) 5mC, (E) H3K9me3 and (F) H3K27me3 after exposure to ATZ. All data are normalized to their corresponding untreated control. Data = mean ± S.E. n > 300 cells. ***: $p < 0.001$. (G–I) t-SNE plots of ATZ-naïve and treated cells based on intensity and texture features of cells immunostained for (G) 5mC, (H) H3K9me3 and (I) H3K27me3. The *t*-SNE space was constructed based on PCA.

treated with 0.3, 3 and 30 ppb of ATZ, respectively as shown in Fig. 4D. Other than overall intensity, we can identify individual foci within nucleus as we demonstrated in our previous publication (Lin et al., 2021). These foci features enable us to carry out foci-specific analysis. Specifically, we can calculate foci intensity, foci distribution, and other correlational features of foci that contribute to the depth of measurements of each cell using a customized CellProfiler pipeline as we described in our previous work (Sánchez et al., 2020). Based on these features, we performed clustering analysis using PCA to determine the separations between ATZ-naïve and treated cells. t-Distributed Stochastic Neighbor Embedding (t-SNE) plots were then constructed for visualizing clusters formed by population of cells treated at different ATZ doses based on these collective features as shown in Fig. 4G. No distinctive clusters can be determined using *k*-means clustering approach, suggesting no good separations between the AZT-naïve and treatment groups based on DNA methylation patterns.

Similar analysis was performed to assess changes in H3K9me3 and H3K27me3 after 96 h exposure to ATZ. In cells stained with H3K9me3 antibody, distinctive clusters are formed inside nucleus and near the nucleus periphery as shown in Fig. 4B (see Fig. S3B (Supporting Information) for more images). The size of foci formed by H3K9me3 are visibly much larger than those formed by 5mC. Relative changes in H3K9me3 induced by ATZ were calculated based on the immunofluorescent intensity and are summarized in Fig. 4E. Exposure to ATZ has resulted in ~50, 70 and 20% loss in

H3K9me3 for cells exposed to 0.3, 3 and 30 ppb of ATZ, respectively. Dimensionality reduction and clustering analysis were subsequently performed to determine the separations between ATZ-naïve and treated cells based on texture features of H3K9me3. No distinctive clusters were identified among ATZ-naïve and ATZ-treated groups (see Fig. 4H).

Cells stained with H3K27me3 antibody exhibited a large bright island near the nucleus periphery corresponding to the barr body presenting in cells with female origin, *i.e.*, SH-SY5Y (Chadwick and Willard 2004; Shenoda et al., 2018). Small foci-like features can be observed within the cell nucleus and nuclear periphery as shown in Fig. 4C. Analysis of fluorescence intensity suggests that ATZ treatment can cause reductions in H3K27me3 levels. ~25, 52 and 20% reduction were observed in cells exposed to 0.3, 3 and 30 ppb of ATZ as shown in Fig. 4F. No clear distinctions can be made among ATZ-naïve and ATZ-treated cells based on its intensity and texture features as shown in Fig. 4I.

To mimic developmental exposure, ATZ-containing culture medium was completely replenished with ATZ-free passaging medium prior to initiating differentiation. Similar epigenetic analysis as described above was performed on Day 14 when most neurons have completed differentiation and are MAP2 positive (MAP2+). Representative images of differentiated SH-SY5Y cells stained with 5mC, H3K9me3 and H3K27me3 antibodies are shown in Fig. 5A, 5B, and 5C, respectively. More images of immuno-stained cells can be found in Fig. S4 (Supporting Information). Since the images of cells at Day 0 and Day 14 were taken on different days, the intensity variations between Day 0 and Day 14 cannot be directly used to estimate the effects of differentiation on epigenome. To address that, we performed continuous culturing using untreated cells and compared the immunofluorescence of 5mC, H3K9me3 and H3K27me3 of cells differentiated and continuously cultured for 14 days as shown in Fig. S5 (Supporting Information). Compared to undifferentiated cells, differentiated SH-SY5Y cells have more established heterochromatin and thus elevated levels of 5mC, H3K9me3, and H3K27me3.

As a result of exposure to ATZ prior to differentiation, differentiated SH-SY5Y cells exhibit significant decrease in 5mC levels with ~85, 30 and 75% reductions for cells exposed to 0.3, 3, and 30 ppb of ATZ, respectively as shown in Fig. 5D. Clustering analysis was carried out and summarized in Fig. 5G. Two major clusters were identified, one consisting primarily of ATZ-naïve cells and cells pre-exposed to 3 ppb of ATZ; and another cluster containing cells exposed to 0.3 and 30 ppb of ATZ. Adaptive LASSO (Least Absolute Shrinkage and Selection Operator) was subsequently performed to identify the features that best distinguish among treatment and control groups (Zou 2006). The top ranked features are summarized in Table S3A (Supporting Information). Higher absolute values of LASSO coefficients suggest larger contributions to distinguishing between different ATZ treatment levels. Among the selected features, intensity and texture features are ranked the highest.

Changes in H3K9me3 and H3K27me3 are quantified using a similar approach with results summarized in Fig. 5E, F, 5H, and 5I. In both cases, the changes in histone methylation induced by exposure to ATZ were compensated for but at different levels. In differentiated cells, decrease in H3K9me3 persists but at a significantly reduced level. ~10, 35 and 30% reductions in H3K9me3 were observed for cells exposed to 0.3, 3 and 30 ppb of ATZ compared to the control as shown in Fig. 5E. No clear clustering, however, can be made among ATZ-naïve and treated groups as shown in Fig. 5H. Changes in H3K27me3 observed right after exposure to ATZ were overcompensated for after the completion of differentiation. There is ~ −2.5, +16 and + 87% change in H3K27me3 for cells exposed to 0.3, 3 and 30 ppb of ATZ, respectively, as shown in Fig. 5F. Surprisingly, we identified two distinctive clusters from cells stained with H3K27me3 antibody, including one cluster that consists primarily of cells exposed to 30 ppb of ATZ and the other containing untreated cells and cells exposed to 0.3 and 3 ppb of ATZ as shown in Fig. 5I. Top-ranked parameters contributing to the definition of the cluster were summarized in Table S3B (Supporting Information). Among them integrated intensity and nuclear periphery intensity were ranked the highest.

3.3. Alterations in epigenetic enzymes after exposure to ATZ

RT-qPCR was performed to determine changes in key epigenetic enzymes that modulate epigenome. Specifically, 5mC is primarily modulated by DNA methyltransferase, including *DNMT1*, *DNMT3A* and *DNMT3B*; and DNA demethylase including *TET1* (Hendrich and Bird 2000; Tahiliani et al., 2009). H3K9me3 is primarily modulated by histone methyltransferase *KMT1A* and histone demethylase *KDM4A* (Lee et al., 2011; Wang et al., 2017). H3K27me3 is co-regulated by histone methyltransferase *EZH2*, and histone demethylases, including *KDM6A* and *KDM6B* (Jiang et al., 2013; Martinez et al., 2018).

Changes in the mRNA level of epigenetic enzymes responsible for 5mC, H3K9me3, and H3K27me3 are summarized in Fig. 6A and B, and 6C, respectively. Exposure to ATZ upregulated the expression level of *DNMT1* (maintenance DNMT) at 3 ppb by ~ 3.2 folds; and *DNMT3B* (*de novo* methyltransferase) at 0.3 and 3 ppb by ~1.8- and 1.9-fold, respectively. No significant changes were detected in *TET1* or *DNMT3A* transcription. After the completion of differentiation, only *DNMT3A* exhibited ~1.7-fold decrease in mRNA level in cells exposed to 0.3 ppb of ATZ. Exposure to ATZ only affects the expression of *KMT1A* (H3K9me3 methyltransferase). Exposure to 3 ppb of ATZ has resulted in ~11.5-fold decrease in *KMT1A* before differentiation. After differentiation, significant changes are observed in cells treated with 30 ppb of ATZ suggesting 1.4-fold increase in transcription. *KDM4A* (H3K9me3 demethylase) does not exhibit significant changes after exposure to ATZ. *EZH2* (H2K27me3 methyltransferase) only exhibited changes after the completion of differentiation. Specifically, the transcription was altered by +1.4-, −1.4- and −1.5-fold at 0.3, 3 and 30 ppb respectively. *KDM6A* (H3K27me3 demethylase) showed ~ 2.9-fold decrease in transcription in cells exposed to 0.3 ppb of ATZ only before differentiation. No significant changes were observed in *KDM6B* either before or after differentiation.

It is also of interest to note the changes in epigenetic enzymes incurred after the completion of differentiation by comparing results from Day 0 and 14. Among them, DNMT1 and KDM6B are the most significantly up-regulated, while KDM6A are the most significantly down-regulated.

4. Discussion

In this work, we focused on low-dose of ATZ exposure (0, 0.3, 3 and 30 ppb) prior to differentiation. We designed our exposure window (see Fig. 1) to mimic developmental exposure to enable assessment of their impact on the development of CNS as shown in Fig. 1. As expected, we observed minimal cytotoxicity at the selected ATZ concentrations. ATZ exposure prior to differentiation can increase the percentage of mature neurons (*MAP2*+), suggesting that ATZ can cause cytoskeletal changes associated with neuronal differentiation. Mature neurons in ATZ-treated samples exhibited different neurite outgrowth patterns. To the best of our knowledge, no prior studies have assessed how pre-differentiation exposure to ATZ can affect the differentiation of SH-SY5Y. The effects of ATZ (12−300 μM) exposure on N27 rat dopaminergic cell, however, were assessed previously (Lin et al., 2013a, 2013b). ATZ

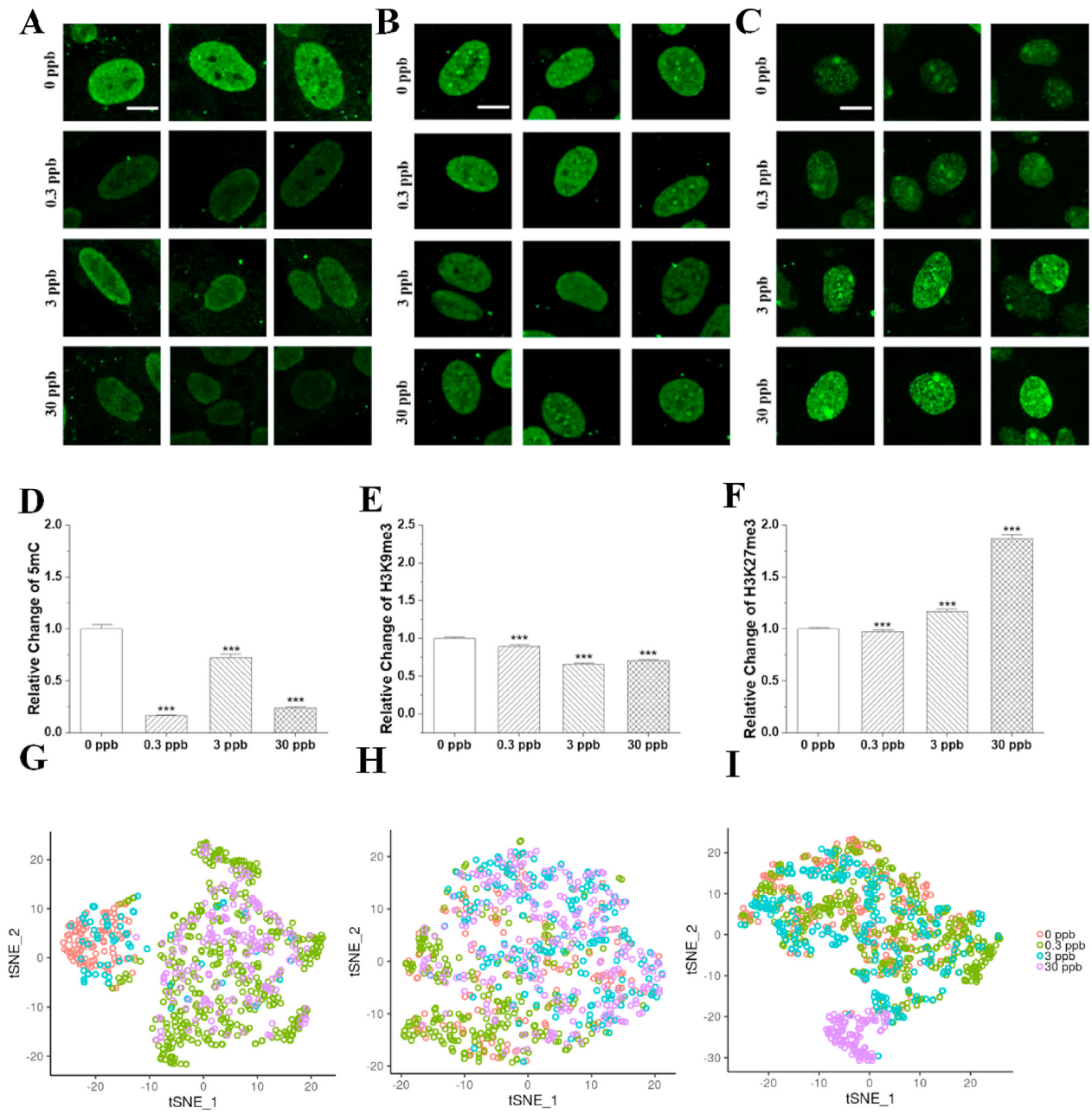

Fig. 5. (A–C) Typical confocal images (z-projected) of differentiated SH-SY5Y neurons (Day 14) stained for (A) 5mC, (B) H3K9me3, and (C) H3K27me3 after 96 h exposure to ATZ prior to differentiation. Scale bar = 5 μm. (D–F) Bar plots of relative change in (D) 5mC, (E) H3K9me3 and (F) H3K27me3 post differentiation. All data is normalized to the corresponding untreated control. Data = mean ± S.E. n > 300 cells. ***: $p < 0.001$. (G–I) t-SNE plots of ATZ-naïve and treated cells based on intensity and texture features of mature neurons immunostained for (G) 5mC, (H) H3K9me3 and (I) H3K27me3. The *t*-SNE space was constructed based on PCA.

exposure was found to alter the morphology of undifferentiated N27 cells. After exposure to ATZ for 48 h, differentiating N27 cells showed increased numbers of neurites and longer neurite length like what we have observed in this study. Different studies have shown that MAP2 is important for retaining neuron morphology, for instance, MAP2-deficient mice have reduced microtubule densities and exhibit alterations in the structure of dendrites, including reductions in dendrite length (Harada et al., 2002). In turn, dendritic complexity determines synaptic density and the size of the receptive field which are associated with memory acquisition, cognitive function, and motor coordination (Lanoue and Cooper 2019). Although we cannot unequivocally determine changes in neuron activity based on the morphological analysis, it is safe to conclude that ATZ-exposure prior to differentiation can cause significant changes in neuron morphology that warrants further studies of neuron activity.

We also characterized changes in molecular markers for PD particularly those involved in *SNCA*-related pathology. Increase in *SNCA* transcription was observed in ATZ treated samples but with changes more significant immediately after exposure (Day 0). Synuclein aggregates were significantly increased in differentiated SH-SY5Y cells that were exposed to 30 ppb of ATZ prior to differentiation after co-treating with dopamine and MPP+. Similar increase in the transcription of *SNCA* was reported in rats exposed to ATZ of 25 or 50 mg/(kg body weight) per day for 3 months (Li et al., 2019) aligning with the general finding of our work. Collectively,

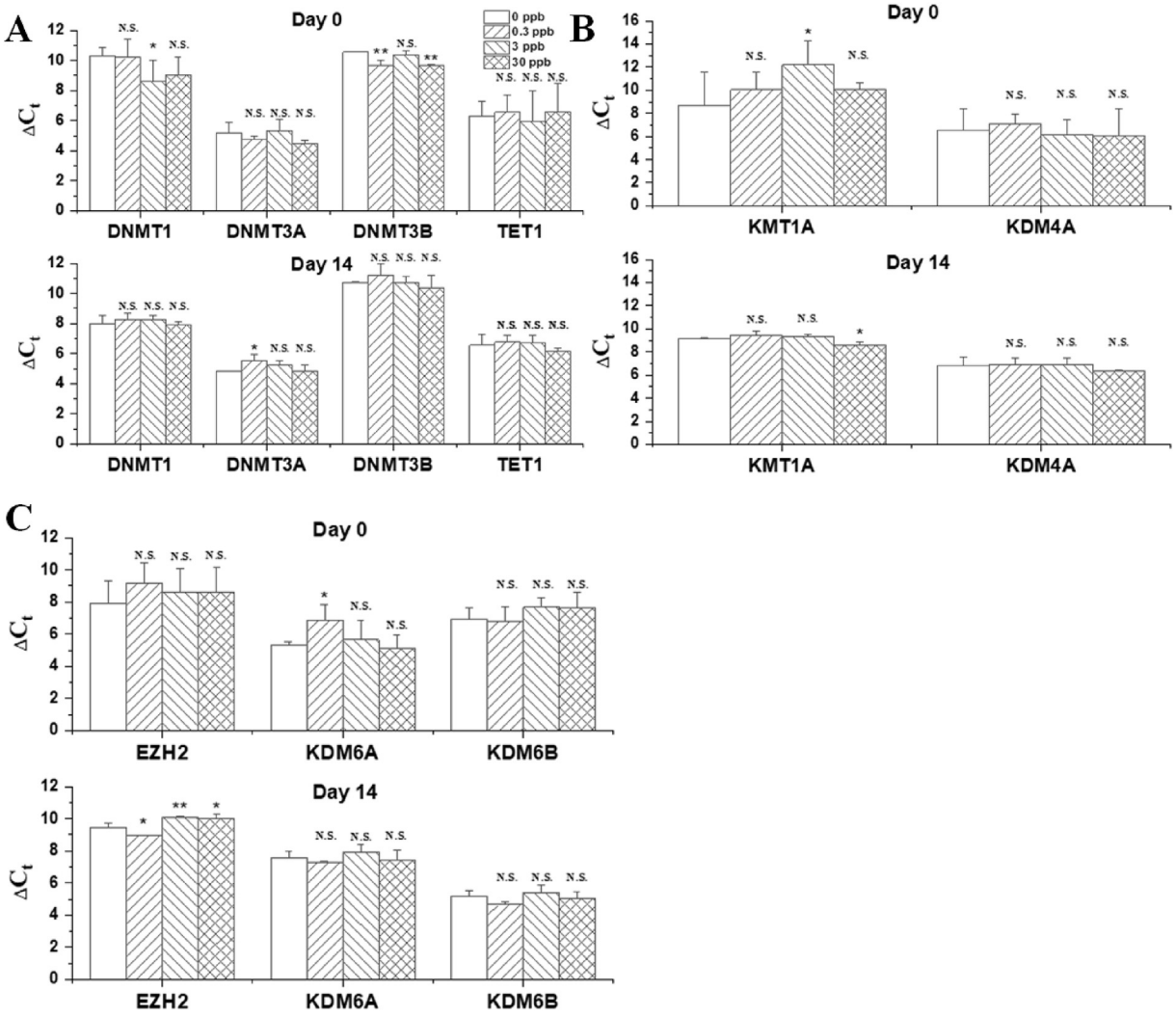

Fig. 6. (A–C) Transcription levels of mRNA coding for epigenetic writer and erasers, assessed immediately after 96 h of exposure to ATZ (top) and 14 days of relaxation and differentiation (bottom). Data are presented as the mean difference in threshold cycle (ΔC_t) between gene of interest and β-actin as internal control. A, B and C depicts changes in epigenetic enzymes responsible for 5mC, H3K9me3, and H3K27me3, respectively. Data = mean ± S.D. n ≥ 3. *: $p < 0.05$; **: $p < 0.01$; and N.S.: not significant.

these findings indicate that exposure to ATZ can alter *SNCA* pathology and potentially increase PD risk after developmental exposure. Increase in *SNCA* expression and α-synuclein aggregates (A11) are commonly accepted molecular hallmarks for PD (Colla et al., 2012; Mohite et al., 2018). The dose dependence as observed in *SNCA* transcription, expression and aggregates, however, do not always agree with each other in our study. This discrepancy can be potentially attributed to the involvement of post-translational mechanism such as phosphorylation and glycosylation. For instance, phosphorylation of serine 129 (S129) in α-synuclein can promote fibril formation and is involved in Lewy body disorders such as Parkinson's Disease (Fujiwara et al., 2002).

Epigenetic assessment immediately after exposure and towards the completion of differentiation confirmed alterations in various silencing markers, including 5mC, H3K9me3, and H3K27me3. In an ATZ-free environment, global levels of 5mC, H3K9me3, and H3K27me3 were increased in differentiated SH-SY5Y compared to undifferentiated ones. Similar trends in the selected markers were reported previously using mouse embryonic stem cells during cell identity establishment (Becker et al., 2016; Juan et al., 2016; Nicetto and Zaret 2019). We thus expect the observed changes as a result of neuronal lineage commitment.

5mC is the most abundant epigenetic modification occurring on DNA and has an established role in gene regulation (Cedar and Razin 2017; Kribelbauer et al., 2017). Compared to other epigenetic modifications, such as histone PTMs, the maintenance and inheritance mechanism of DNA methylation are well-established (Wang et al., 2016; Yao et al., 2016). In our study, exposure to ATZ is shown to immediately increase 5mC levels along with increase in *DNMT1* and *DNMT3B* expression at selected doses and thus partially accounting for the changes that we observed on Day 0. After differentiation, alterations in epigenetic enzymes responsible for DNA methylation are almost completely recovered with the only exception of *DNMT3A* at 0.3 ppb. These results collectively suggest non-linear dependence on ATZ doses in shaping DNA methylome in exposed cells. Similar non-linear dependent DNA methylation changes induced by exposure to ATZ have been reported previously in the liver tissues of common carp exposed to ATZ (Wang et al., 2014; Xing et al., 2015). Hypermethylation in 5 mC has been previously reported in SH-SY5Y cells with chronic exposure of manganese (Mn) globally and on specific loci (i.e. *PINK1* and *PARK2*) which might contribute to the onset of PD (Tarale et al., 2017). DNA hypomethylation has also been previous reported for differentiated SH-SY5Y exposed to all-*trans*-retinoic acid (Stallings et al., 2011)

and PM 2.5 (Wei et al., 2016).

H3K9me3 is a repressive marker commonly found in constitutively silenced chromatin. Different roles of H3K9me3 have been associated with neuron functions, including hippocampal memory (Snigdha et al., 2016) and cortical development (Aucott et al., 2008). H3K9me3 levels increase when differentiating hESC H9 into neural stem cells facilitating commitment to specific neuronal lineages (Golebiewska et al., 2009). Reductions in H3K9me3 were observed immediately after exposure to ATZ and persisted at a significantly reduced level after removal of ATZ and completion of differentiation. Decrease in histone methyltransferase (*KMT1A*) can at least partially account for decrease in H3K9me3 levels observed immediately after exposure. Our results aligned with previous reports where human embryonic HEK293T cells exposed to ATZ (3 and 30 ppb) exhibit a relative drop in H3K9me3 levels of ~14% and 29%, respectively (Sánchez et al., 2020).

H3K27me3 is a bi-valent epigenetic marker commonly found in facultative heterochromatin regions. Aberrant expression of H3K27me3 has been associated with various neurodegeneration diseases. For example, reductions in H3K27me3 caused by loss of EZH1/2 can induce cell apoptosis in D1 and D2 dopamine receptor-positive neurons (von Schimmelmann et al., 2016). Increase in H3K27me3 induced by upregulating EZH2 can cause neurodegeneration of cerebellum in ataxia-telangiectasia (Li et al., 2013). H3K27me3 is decreased when ESC is differentiated into neuronal stem cells (Adefuin et al., 2014), but increased when neural stem cells are differentiated into neurons of specific lineages (Liu et al., 2017). Like H3K9me3, H3K27me3 was significantly reduced after exposure to ATZ. Compensation effects were observed similarly in H3K27me3. As a result, a significant increase in H3K27me3 was observed in differentiated SH-SY5Y cells, particularly for cells that have been exposed to 3 and 30 ppb of ATZ. The transcriptional level change of epigenetic enzymes responsible for H3K27me3 fails to account for the observed changes in H3K27me3. To the best of our knowledge, there are no previous studies examining ATZ effects on H3K27me3 levels and distribution.

One common theme that is observed in epigenetic features, and the selected *SNCA* molecular marker is that the exposure effects are commonly compensated for after the removal of exposure source and the completion of differentiation. Over-compensation is also observed and can result in larger deviations from the ATZ-naïve cells as observed in 5mC and H3K27me3 (30 ppb) which may be the direct cause of neurotoxicity arising at a later life stage. To the best of our knowledge, there are no prior studies assessing the persistency of transcription and epigenome changes after exposure to ATZ. The observed compensatory effects, however, aligns with what was expected from cells when restoring homeostasis. Furthermore, our results suggest that ATZ-treated cells exhibit lower levels of permanent repressive markers, such as 5mC and H3K9me3, and higher levels of facultative repressive markers, such as H3K27me3 while maintaining cell viability. H3K27me3 thus seems to partially compensate for the loss in 5mC and H3K9me3 to retain cell functionality. Similar findings were observed in mouse embryonic stem cells deficient in DNA and H3K9me3 (Saksouk et al., 2015). As a surviving strategy, these cells were enriched in H3K27me3. Similarly, the knockout of the epigenetic regulator *Uhrf1*, essential for DNA methylation maintenance, in hepatocytes can lead to increased abundance and re-distribution of H3K27me3 markers (Wang et al., 2019). Our results are thus in line with these observations suggesting that exposure to ATZ during a developmental window can disrupt the formation of constitutive heterochromatins but compensated for that by the formation of facultative chromatin enriched in H3K27me3. As a result, we would expect minimal transcriptome changes in short-term but increased genome instability as other exposure events influence the cellular health. Overall, our results provide evidence of epigenome changes and their persistence induced by an early developmental exposure to ATZ in an *in vitro* model.

5. Conclusions

Collectively, exposure to low-dose of ATZ can alter epigenetic features as well as molecular markers characteristic of PD. After the cessation of exposure and completion of differentiation, changes in epigenome remain but in a compensated manner. Among the selected epigenetic markers, we found that 5mC and H3K27me3 changes are overcompensated while changes in H3K9me3 persist at a reduced magnitude. These results collectively suggest that ATZ-exposed cells could have disrupted the formation of constitutive heterochromatin that was compensated by increased levels of facultative heterochromatin enriched in H3K27me3. Meanwhile, *SNCA*-related PD markers were also altered suggesting PD-like pathology. Our results thus suggest that developmental exposure to low dose of ATZ can induce long-term neurotoxicity via altered epigenome.

Authorship statement

Conceptualization: JX, LL, JLF, CY Methodology: JX, LL, CY Formal Analysis: JX, LL, CB Investigation: JX, LL Data Curation: JX, LL, OS, CB Writing – Original Draft: JX, OS, CY Writing – Review & Editing: JX, LL, OS, JLF, CY

Funding

This work was supported by National Science Foundation [CBET-1512285, CBET-1705560 & EF-1935226].

The authors declare they have no actual or potential competing financial interests.

Declaration of competing interest

The authors declare that they have no known competing financial interests or personal relationships that could have appeared to influence the work reported in this paper.

Appendix A. Supplementary data

Supplementary data to this article can be found online at https://doi.org/10.1016/j.envpol.2020.116379.

References

Adefuin, A.M.D., Kimura, A., Noguchi, H., Nakashima, K., Namihira, M., 2014. Epigenetic mechanisms regulating differentiation of neural stem/precursor cells. Epigenomics 6 (6), 637–649.

Aucott, R., Bullwinkel, J.r., Yu, Y., Shi, W., Billur, M., Brown, J.P., Menzel, U., Kioussis, D., Wang, G., Reisert, I., 2008. HP1-β is required for development of the cerebral neocortex and neuromuscular junctions. J. Cell Biol. 183 (4), 597–606.

Becker, J.S., Nicetto, D., Zaret, K.S., 2016. H3K9me3-Dependent heterochromatin: barrier to cell fate changes. Trends Genet. 32 (1), 29–41.

Cedar, H., Razin, A., 2017. Annotating the genome by DNA methylation. Int. J. Dev. Biol. 61 (3–4-5), 137–148.

Chadwick, B.P., Willard, H.F., 2004. Multiple spatially distinct types of facultative heterochromatin on the human inactive X chromosome. Proc. Natl. Acad. Sci. Unit. States Am. 101 (50), 17450–17455.

Cheremisinoff, N.P., Cheremisinoff, N.P., Rosenfeld, P.E., 2011. In: 4 - Atrazine. Handbook of Pollution Prevention and Cleaner Production: Best Practices in the Agrochemical Industry. William Andrew Publishing, Oxford, pp. 215–231.

Chun, H.S., Gibson, G.E., DeGiorgio, L.A., Zhang, H., Kidd, V.J., Son, J.H., 2001. Dopaminergic cell death induced by MPP(+), oxidant and specific neurotoxicants shares the common molecular mechanism. J. Neurochem. 76 (4), 1010–1021.

Coban, A., Filipov, N.M., 2007. Dopaminergic toxicity associated with oral exposure

to the herbicide atrazine in juvenile male C57BL/6 mice. J. Neurochem. 100 (5), 1177–1187.
Colla, E., Jensen, P.H., Pletnikova, O., Troncoso, J.C., Glabe, C., Lee, M.K., 2012. Accumulation of toxic α-synuclein oligomer within endoplasmic reticulum occurs in α-synucleinopathy in vivo. J. Neurosci. 32 (10), 3301–3305.
EPA., U. S., 2002. List of Contaminants and Their MCLs. . EPA 816-F-02-013. U.S. Environmental Protection Agency, Washington, DC.
EPA., U. S., 2006. Decision Documents for Atrazine.
Fujiwara, H., Hasegawa, M., Dohmae, N., Kawashima, A., Masliah, E., Goldberg, M.S., Shen, J., Takio, K., Iwatsubo, T., 2002. alpha-Synuclein is phosphorylated in synucleinopathy lesions. Nat. Cell Biol. 4 (2), 160–164.
Gebremedhin, K.G., Rademacher, D.J., 2016. Histone H3 acetylation in the post-mortem Parkinson's disease primary motor cortex. Neurosci. Lett. 627, 121–125.
Gianessi, P., Marcelli, M.B., 2000. Pesticide Use in U.S. Crop Production: 1997. National Summary Report.
Giusi, G., Facciolo, R.M., Canonaco, M., Alleva, E., Belloni, V., Dessi'-Fulgheri, F., Santucci, D., 2005. The endocrine disruptor atrazine accounts for a dimorphic somatostatinergic neuronal expression pattern in mice. Toxicol. Sci. 89 (1), 257–264.
Goldberg, A.D., Allis, C.D., Bernstein, E., 2007. Epigenetics: a landscape takes shape. Cell 128 (4), 635–638.
Golebiewska, A., Atkinson, S.P., Lako, M., Armstrong, L., 2009. Epigenetic landscaping during hESC differentiation to neural cells. Stem Cell. 27 (6), 1298–1308.
Hao, C., Gely-Pernot, A., Kervarrec, C., Boudjema, M., Becker, E., Khil, P., Tevosian, S., Jégou, B., Smagulova, F., 2016. Exposure to the widely used herbicide atrazine results in deregulation of global tissue-specific RNA transcription in the third generation and is associated with a global decrease of histone trimethylation in mice. Nucleic Acids Res. 44 (20), 9784–9802.
Harada, A., Teng, J., Takei, Y., Oguchi, K., Hirokawa, N., 2002. MAP2 is required for dendrite elongation, PKA anchoring in dendrites, and proper PKA signal transduction. J. Cell Biol. 158 (3), 541–549.
Hendrich, B., Bird, A., 2000. Mammalian methyltransferases and methyl-CpG-binding domains: proteins involved in DNA methylation. Curr. Top. Microbiol. Immunol. 249, 55–74.
Horzmann, K.A., Lin, L.F., Taslakjian, B., Yuan, C., Freeman, J.L., 2020. Embryonic atrazine exposure and later in life behavioral and brain transcriptomic, epigenetic, and pathological alterations in adult male zebrafish. Cell Biol. Toxicol.
Jiang, W., Wang, J., Zhang, Y., 2013. Histone H3K27me3 demethylases KDM6A and KDM6B modulate definitive endoderm differentiation from human ESCs by regulating WNT signaling pathway. Cell Res. 23 (1), 122–130.
Juan, Aster H., Wang, S., Ko, Kyung D., Zare, H., Tsai, P.-F., Feng, X., Vivanco, Karinna O., Ascoli, Anthony M., Gutierrez-Cruz, G., Krebs, J., Sidoli, S., Knight, Adam L., Pedersen, Roger A., Garcia, Benjamin A., Casellas, R., Zou, J., Sartorelli, V., 2016. Roles of H3K27me2 and H3K27me3 examined during fate specification of embryonic stem cells. Cell Rep. 17 (5), 1369–1382.
Kribelbauer, J.F., Laptenko, O., Chen, S., Martini, G.D., Freed-Pastor, W.A., Prives, C., Mann, R.S., Bussemaker, H.J., 2017. Quantitative analysis of the DNA methylation sensitivity of transcription factor complexes. Cell Rep. 19 (11), 2383–2395.
Lanoue, V., Cooper, H.M., 2019. Branching mechanisms shaping dendrite architecture. Dev. Biol. 451 (1), 16–24.
Lee, M.H., Jothi, M., Gudkov, A.V., Mal, A.K., 2011. Histone methyltransferase KMT1A restrains entry of alveolar rhabdomyosarcoma cells into a myogenic differentiated state. Canc. Res. 71 (11), 3921–3931.
Li, J., Hart, R.P., Mallimo, E.M., Swerdel, M.R., Kusnecov, A.W., Herrup, K., 2013. EZH2-mediated H3K27 trimethylation mediates neurodegeneration in ataxia-telangiectasia. Nat. Neurosci. 16 (12), 1745–1753.
Li, Y.S., He, X., Ma, K., Wu, Y.P., Li, B.X., 2015. The effect of exposure to atrazine on dopaminergic development in pubertal male SD rats. Birth Defects Res B Dev Reprod Toxicol 104 (5), 184–189.
Li, B., Jiang, Y., Xu, Y., Li, Y., Li, B., 2019. Identification of miRNA-7 as a regulator of brain-derived neurotrophic factor/α-synuclein axis in atrazine-induced Parkinson's disease by peripheral blood and brain microRNA profiling. Chemosphere 233, 542–548.
Lin, Z., Dodd, C.A., Filipov, N.M., 2013a. Differentiation state-dependent effects of in vitro exposure to atrazine or its metabolite diaminochlorotriazine in a dopaminergic cell line. Life Sci. 92 (1), 81–90.
Lin, Z., Dodd, C.A., Filipov, N.M., 2013b. Short-term atrazine exposure causes behavioral deficits and disrupts monoaminergic systems in male C57BL/6 mice. Neurotoxicol. Teratol. 39, 26–35.
Lin, Z., Dodd, C.A., Xiao, S., Krishna, S., Ye, X., Filipov, N.M., 2014. Gestational and lactational exposure to atrazine via the drinking water causes specific behavioral deficits and selectively alters monoaminergic systems in C57BL/6 mouse dams, juvenile and adult offspring. Toxicol. Sci. 141 (1), 90–102.
Lin, L., Xie, J., Sanchez, O.F., Bryan, C., Freeman, J., Yuan, C., 2020. Low dose lead exposure induces alterations on heterochromatin hallmarks persisting through SH-SY5Y cell differentiation. bioRxiv: 2020, 2007.2027.224246.
Lin, L.F., Xie, J., Sánchez, O.F., Bryan, C., Freeman, J.L., Yuan, C., 2021. Low dose lead exposure induces alterations on heterochromatin hallmarks persisting through SH-SY5Y cell differentiation. Chemosphere 264, 128486.
Liu, J., Wu, X., Zhang, H., Pfeifer, G.P., Lu, Q., 2017. Dynamics of RNA polymerase II pausing and bivalent histone H3 methylation during neuronal differentiation in brain development. Cell Rep. 20 (6), 1307–1318.
Martinez, D., Zuhdi, N., Reyes, M., Ortega, B., Giovannone, D., Lee, V.M., de Bellard, M.E., 2018. Screen for Slit/Robo signaling in trunk neural cells reveals new players. Gene Expr. Patterns 28, 22–33.
McBirney, M., King, S.E., Pappalardo, M., Houser, E., Unkefer, M., Nilsson, E., Sadler-Riggleman, I., Beck, D., Winchester, P., Skinner, M.K., 2017. Atrazine induced epigenetic transgenerational inheritance of disease, lean phenotype and sperm epimutation pathology biomarkers. PloS One 12 (9) e0184306-e0184306.
Mohite, G.M., Dwivedi, S., Das, S., Kumar, R., Paluri, S., Mehra, S., Ruhela, N., Jha, A.S.N.N., Maji, S.K., 2018. Parkinson's disease associated α-synuclein familial mutants promote dopaminergic neuronal death in Drosophila melanogaster. ACS Chem. Neurosci. 9 (11), 2628–2638.
Moore, L.D., Le, T., Fan, G., 2013. DNA methylation and its basic function. Neuropsychopharmacology : official publication of the American College of Neuropsychopharmacology 38 (1), 23–38.
Mozzetta, C., Boyarchuk, E., Pontis, J., Ait-Si-Ali, S., 2015. Sound of silence: the properties and functions of repressive Lys methyltransferases. Nat. Rev. Mol. Cell Biol. 16 (8), 499–513.
Munger, R., Isacson, P., Hu, S., Burns, T., Hanson, J., Lynch, C.F., Cherryholmes, K., Van Dorpe, P., Hausler Jr., W.J., 1997. Intrauterine growth retardation in Iowa communities with herbicide-contaminated drinking water supplies. Environ. Health Perspect. 105 (3), 308–314.
Nicetto, D., Zaret, K.S., 2019. Role of H3K9me3 heterochromatin in cell identity establishment and maintenance. Curr. Opin. Genet. Dev. 55, 1–10.
Park, G., Tan, J., Garcia, G., Kang, Y., Salvesen, G., Zhang, Z., 2016. Regulation of histone acetylation by autophagy in Parkinson disease. J. Biol. Chem. 291 (7), 3531–3540.
Raja, S., Ravikrishna, R., Kommalapati, R., Valsaraj, K., 2005. Monitoring of fogwater chemistry in the gulf coast urban industrial corridor: baton Rouge (Louisiana). Environ. Monit. Assess. 110 (1–3), 99–120.
Rawlik, K., Rowlatt, A., Tenesa, A., 2016. Imputation of DNA methylation levels in the brain implicates a risk factor for Parkinson's disease. Genetics 204 (2), 771–781.
Rohr, J.R., McCoy, K.A., 2010. A qualitative meta-analysis reveals consistent effects of atrazine on freshwater fish and amphibians. Environ. Health Perspect. 118 (1), 20–32.
Saksouk, N., Simboeck, E., Déjardin, J., 2015. Constitutive heterochromatin formation and transcription in mammals. Epigenet. Chromatin 8 (1), 3.
Sánchez, O.F., Mendonca, A., Min, A., Liu, J., Yuan, C., 2019. Monitoring histone methylation (H3K9me3) changes in live cells. ACS Omega 4 (8), 13250–13259.
Sánchez, O.F., Lin, L., Bryan, C.J., Xie, J., Freeman, J.L., Yuan, C., 2020. Profiling epigenetic changes in human cell line induced by atrazine exposure. Environ. Pollut. 258, 113712.
Schmidel, A.J., Assmann, K.L., Werlang, C.C., Bertoncello, K.T., Francescon, F., Rambo, C.L., Beltrame, G.M., Calegari, D., Batista, C.B., Blaser, R.E., Roman Júnior, W.A., Conterato, G.M.M., Piato, A.L., Zanatta, L., Magro, J.D., Rosemberg, D.B., 2014. Subchronic atrazine exposure changes defensive behaviour profile and disrupts brain acetylcholinesterase activity of zebrafish. Neurotoxicol. Teratol. 44, 62–69.
Shenoda, B.B., Tian, Y., Alexander, G.M., Aradillas-Lopez, E., Schwartzman, R.J., Ajit, S.K., 2018. miR-34a-mediated regulation of XIST in female cells under inflammation. J. Pain Res. 11, 935.
Shipley, M.M., Mangold, C.A., Szpara, M.L., 2016. Differentiation of the SH-SY5Y human neuroblastoma cell line. JoVE : JoVE 108, 53193-53193.
Simpkins, J.W., Swenberg, J.A., Weiss, N., Brusick, D., Eldridge, J.C., Stevens, J.T., Handa, R.J., Hovey, R.C., Plant, T.M., Pastoor, T.P., Breckenridge, C.B., 2011. Atrazine and breast cancer: a framework assessment of the toxicological and epidemiological evidence. Toxicol. Sci. : an official journal of the Society of Toxicology 123 (2), 441–459.
Snigdha, S., Prieto, G.A., Petrosyan, A., Loertscher, B.M., Dieskau, A.P., Overman, L.E., Cotman, C.W., 2016. H3K9me3 inhibition improves memory, promotes spine formation, and increases BDNF levels in the aged Hippocampus. J. Neurosci. : the official journal of the Society for Neuroscience 36 (12), 3611–3622.
Song, X.-Y., Li, J.-N., Wu, Y.-P., Zhang, B., Li, B.-X., 2015. Atrazine causes autophagy- and apoptosis-related neurodegenerative effects in dopaminergic neurons in the rat nigrostriatal dopaminergic system. Int. J. Mol. Sci. 16 (6), 13490–13506.
Stallings, R.L., Foley, N.H., Bray, I.M., Das, S., Buckley, P.G., 2011. MicroRNA and DNA methylation alterations mediating retinoic acid induced neuroblastoma cell differentiation. Seminars in Cancer Biology. Elsevier.
Sun, Y., Li, Y.S., Yang, J.W., Yu, J., Wu, Y.P., Li, B.X., 2014. Exposure to atrazine during gestation and lactation periods: toxicity effects on dopaminergic neurons in offspring by downregulation of Nurr1 and VMAT2. Int. J. Mol. Sci. 15 (2), 2811–2825.
Tahiliani, M., Koh, K.P., Shen, Y., Pastor, W.A., Bandukwala, H., Brudno, Y., Agarwal, S., Iyer, L.M., Liu, D.R., Aravind, L., Rao, A., 2009. Conversion of 5-methylcytosine to 5-hydroxymethylcytosine in mammalian DNA by MLL partner TET1. Science 324 (5929), 930–935.
Tarale, P., Sivanesan, S., Daiwile, A.P., Stöger, R., Bafana, A., Naoghare, P.K., Parmar, D., Chakrabarti, T., Kannan, K., 2017. Global DNA methylation profiling of manganese-exposed human neuroblastoma SH-SY5Y cells reveals epigenetic alterations in Parkinson's disease-associated genes. Arch. Toxicol. 91 (7), 2629–2641.
von Schimmelmann, M., Feinberg, P.A., Sullivan, J.M., Ku, S.M., Badimon, A., Duff, M.K., Wang, Z., Lachmann, A., Dewell, S., Ma'ayan, A., 2016. Polycomb repressive complex 2 (PRC2) silences genes responsible for neurodegeneration. Nat. Neurosci. 19 (10), 1321–1330.
Vonberg, D., Hofmann, D., Vanderborght, J., Lelickens, A., Köppchen, S., Pütz, T., Burauel, P., Vereecken, H., 2014. Atrazine soil core residue analysis from an agricultural field 21 Years after its ban. J. Environ. Qual. 43 (4), 1450–1459.

Walters, J.L., Lansdell, T.A., Lookingland, K.J., Baker, L.E., 2015. The effects of gestational and chronic atrazine exposure on motor behaviors and striatal dopamine in male Sprague-Dawley rats. Toxicol. Appl. Pharmacol. 289 (2), 185–192.
Wang, C., Zhang, Z., Yao, H., Zhao, F., Wang, L., Wang, X., Xing, H., Xu, S., 2014. Effects of atrazine and chlorpyrifos on DNA methylation in the liver, kidney and gill of the common carp (Cyprinus carpio L.). Ecotoxicol. Environ. Saf. 108, 142–151.
Wang, Z., Tang, B., He, Y., Jin, P., 2016. DNA methylation dynamics in neurogenesis. Epigenomics 8 (3), 401–414.
Wang, X., Wang, S., Yao, G., Yu, D., Chen, K., Tong, Q., Ye, L., Wu, C., Sun, Y., Li, H., Hermann, D.M., Doeppner, T.R., Jin, F., Dai, Y., Wu, J., 2017. Identification of the histone lysine demethylase KDM4A/JMJD2A as a novel epigenetic target in M1 macrophage polarization induced by oxidized LDL. Oncotarget 8 (70), 114442–114456.
Wang, S., Zhang, C., Hasson, D., Desai, A., SenBanerjee, S., Magnani, E., Ukomadu, C., Lujambio, A., Bernstein, E., Sadler, K.C., 2019. Epigenetic compensation promotes liver regeneration. Dev. Cell 50 (1), 43–56 e46.
Wei, H., Liang, F., Meng, G., Nie, Z., Zhou, R., Cheng, W., Wu, X., Feng, Y., Wang, Y., 2016. Redox/methylation mediated abnormal DNA methylation as regulators of ambient fine particulate matter-induced neurodevelopment related impairment in human neuronal cells. Sci. Rep. 6 (1), 33402.
Wen, K.-x., Miliç, J., El-Khodor, B., Dhana, K., Nano, J., Pulido, T., Kraja, B., Zaciragic, A., Bramer, W.M., Troup, J., Chowdhury, R., Ikram, M.A., Dehghan, A., Muka, T., Franco, O.H., 2016. The role of DNA methylation and histone modifications in neurodegenerative diseases: a systematic review. PloS One 11 (12), e0167201.
Wiles, E.T., Selker, E.U., 2017. H3K27 methylation: a promiscuous repressive chromatin mark. Curr. Opin. Genet. Dev. 43, 31–37.
Wirbisky, S.E., Weber, G.J., Sepúlveda, M.S., Xiao, C., Cannon, J.R., Freeman, J.L., 2015. Developmental origins of neurotransmitter and transcriptome alterations in adult female zebrafish exposed to atrazine during embryogenesis. Toxicology 333, 156–167.
Wirbisky-Hershberger, S.E., Sanchez, O.F., Horzmann, K.A., Thanki, D., Yuan, C., Freeman, J.L., 2017. Atrazine exposure decreases the activity of DNMTs, global DNA methylation levels, and dnmt expression. Food Chem. Toxicol. : an international journal published for the British Industrial Biological Research Association 109 (Pt 1), 727–734.
Wysocka, J., Swigut, T., Xiao, H., Milne, T.A., Kwon, S.Y., Landry, J., Kauer, M., Tackett, A.J., Chait, B.T., Badenhorst, P., Wu, C., Allis, C.D., 2006. A PHD finger of NURF couples histone H3 lysine 4 trimethylation with chromatin remodelling. Nature 442 (7098), 86–90.
Xicoy, H., Wieringa, B., Martens, G.J.M., 2017. The SH-SY5Y cell line in Parkinson's disease research: a systematic review. Mol. Neurodegener. 12 (1), 10.
Xie, H.-r., Hu, L.-s., Li, G.-y., 2010. SH-SY5Y human neuroblastoma cell line: in vitrocell model of dopaminergic neurons in Parkinson's disease. Chinese Med J 123 (8), 1086–1092.
Xing, H., Wang, C., Wu, H., Chen, D., Li, S., Xu, S., 2015. Effects of atrazine and chlorpyrifos on DNA methylation in the brain and gonad of the common carp. Comp. Biochem. Physiol. C Toxicol. Pharmacol. 168, 11–19.
Yamakawa, K., Izumi, Y., Takeuchi, H., Yamamoto, N., Kume, T., Akaike, A., Takahashi, R., Shimohama, S., Sawada, H., 2010. Dopamine facilitates α-synuclein oligomerization in human neuroblastoma SH-SY5Y cells. Biochem. Biophys. Res. Commun. 391 (1), 129–134.
Yao, B., Christian, K.M., He, C., Jin, P., Ming, G.-L., Song, H., 2016. Epigenetic mechanisms in neurogenesis. Nat. Rev. Neurosci. 17 (9), 537–549.
Young, J.I., Sivasankaran, S.K., Wang, L., Ali, A., Mehta, A., Davis, D.A., Dykxhoorn, D.M., Petito, C.K., Beecham, G.W., Martin, E.R., Mash, D.C., Pericak-Vance, M., Scott, W.K., Montine, T.J., Vance, J.M., 2019. Genome-wide brain DNA methylation analysis suggests epigenetic reprogramming in Parkinson disease. Neurol Genet 5 (4), e342.
Zou, H., 2006. The adaptive lasso and its oracle properties. J. Am. Stat. Assoc. 101 (476), 1418–1429.